

pubs.acs.org/JPCC Article

Stability of Pd Islands on Ag(111) and Au(111)

Buddhika S. A. Gedara and Michael Trenary*



Cite This: J. Phys. Chem. C 2023, 127, 516–522



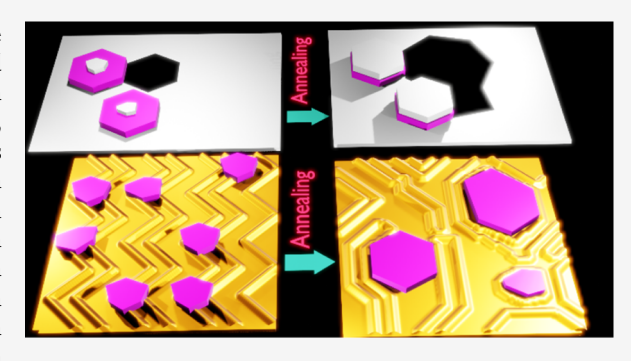
ACCESS I

Metrics & More

Article Recommendations

Supporting Information

ABSTRACT: Scanning tunneling microscopy was used to compare the evolution with time and annealing temperature of the structure of Pd islands formed after room-temperature (RT) deposition of Pd on Ag(111) and Au(111). Although silver and gold share many properties, their clean (111) surfaces have distinctly different structures, and this leads to distinctly different behavior following Pd deposition. On Ag(111), large Pd islands form and become capped by Ag atoms with the simultaneous formation of vacancy pits on the Ag(111) surface. On Au(111), smaller Pd islands form for comparable Pd coverages. In contrast to Ag(111), much less capping of Pd by Au atoms occurs on the Au(111) surface at RT and no vacancy pits were observed. Upon annealing to 340 K, 98% of the Pd islands were capped by Ag atoms on



Ag(111), whereas less than 4% of Pd islands on Au(111) were covered by surface Au atoms, but again without forming vacancy pits. Upon further annealing to 470 K, Pd diffuses into the subsurface of both Ag(111) and Au(111). The contrasting behavior is attributed to the herringbone reconstruction on Au(111), which provides sites with higher binding energies for Pd atoms, whereas such sites are not present on Ag(111).

■ INTRODUCTION

An understanding of the atomic structure of Pd deposited onto the surfaces of silver and gold is important because bimetallic catalysts based on these metals are widely used for a variety of processes. For example, PdAu alloys are used in oxidation of toluene, electrochemical oxidation in fuel cells, removal of chlorine from organic compounds,3 and several other applications as listed by Baber et al.4 Surface science studies have revealed that the activity is often governed by the arrangement of the surface metal atoms. It has been found that Pd monomers are required for CO adsorption and oxidation, whereas Pd dimers are required for hydrogen adsorption.² Moreover, Baber et al. observed that Pd islands are required for a significant uptake of H on a Pd/Au(111) surface.⁴ Furthermore, Ouyang et al. demonstrated that a Pd singleatom alloy is selective to acetaldehyde and hydrogen, whereas Pd clusters lead to the formation of CO, ethyl acetate, and CH₄ as byproducts in the ethanol dehydrogenation reaction.⁵

Catalysts based on PdAg alloys are used in many reactions including selective hydrogenation of acrolein, 6,7 nitrate and nitrite reduction in water, 8,9 formic acid oxidation, 10 hydrogenation of CO_2 to formic acid, 11,12 and selective methylation of aromatic amines. 13 The geometry of the active metal governs the activity of this bimetallic catalyst as well. For instance, H atom spillover does not occur at isolated Pd atoms on $\mathrm{Ag}(111)$, 14 whereas Pd islands on $\mathrm{Ag}(111)$ can dissociate H_2 into H atoms that can spill over to Ag sites. 15

Previously, we reported a scanning tunneling microscopy (STM) study of the evolution of the structure of Pd islands on

Ag(111) with time and upon annealing to different temperatures. 16 In this study, we compare and contrast the behavior of Pd on the Au(111) and Ag(111) surfaces. The thermodynamics of Pd on Ag(111) and Au(111) favors diffusion of Pd into the bulk of the substrate because of the higher surface free energy of Pd (2.0 J m⁻²) than that of Ag (1.3 J m⁻²) and Au (1.6 J m⁻²).¹⁷ These differences in surface free energies lead, for example, to Au segregation to the surface of Au₃Pd(110). 18 Christensen et al. have considered in detail the thermodynamics of surface phase diagrams of binary metal alloys and calculated segregation energies for Pd impurities in Ag and Au hosts to be 0.35 and 0.15 eV/atom, respectively, confirming that thermodynamics favors Pd diffusion into the bulk of both Ag and Au. 19 Although Ag and Au have lower surface free energies than Pd and are both relatively inert metals with similar chemical properties, the Ag(111) surface has a simple unreconstructed structure, whereas Au(111) has the herringbone reconstruction. Giesen has provided a detailed literature review of studies on the stability and dynamics of defects, such as steps, kinks, vacancies, and adatoms, and of monolayer islands on metal surfaces.²⁰ For the most part, the review focuses on pure metals, unlike the bimetallic systems

Received: July 29, 2022 Revised: December 7, 2022 Published: December 23, 2022





studied here. One significant difference between Ag(111) and Au(111) is that the step edges of the former surface appear frizzy in STM images. However, steps and the edges of monolayer Au islands on Au(111) appear relatively sharp, indicating slower rates for atom attachment and detachment processes on Au(111). These differences in the properties of Ag(111) and Au(111) surfaces lead to a distinctly different behavior of Pd deposited onto the two surfaces.

A variety of metals deposited on Au(111) have been studied, including Co,²³ Cr,²⁴ Fe,²⁵ Mn,²⁶ Mo,²⁷ Ni,^{28–31} Pd,^{4,32–35} Pt,³⁶ Rh,^{37,38} Sn,³⁹ Ti,⁴⁰ and Zn.^{41,42} Of most relevance to the present study are the STM results on the nucleation and growth of Pd islands on Au(111) by Stephenson et al.³³ and Casari et al.³⁴ Although these studies focused on the nucleation of Pd islands at room temperature (RT), they did not report on the stability of Pd islands as a function of annealing temperature as we do here. Baber et al. also studied Pd on Au(111) using STM, and they discovered that the herringbone structure of Au(111) provided the entry sites for the incorporation of Pd atoms into the Au lattice and that the extent of mixing of Pd atoms with the Au surface depended on temperature.³⁵ Furthermore, they found that the electronic structure of surface and subsurface Pd atoms was almost identical to that of the surrounding Au atoms.³⁵ In a separate study of hydrogen interaction with Pd/Au(111) and Pd/ Cu(111), Baber et al. showed with STM images of Pd on Au(111) obtained at 450 K that the islands disappear as Pd diffuses across the Au terraces to nearby edge dislocations or to steps where alloying occurs.⁴ They also showed with lowtemperature atomically resolved STM images the effect of deposition temperature on the incorporation of Pd atoms into the Au(111) surface layer and how this process preferentially occurs at 370 K by replacement of Au atoms at edge dislocations. Despite the extensive previous studies of Pd deposited onto the Ag(111) and Au(111) surfaces, the work presented here focuses on the stability of Pd islands that form at low Pd coverages on Au(111). This is an important aspect as our previous work on Pd/Ag(111) demonstrated that even at RT, Pd islands become encapsulated by Ag atoms, ¹⁶ a behavior that had previously been reported only after annealing the surface to higher temperatures. 43 It is therefore important to explore whether a similar behavior might occur for Pd/ Au(111), which required monitoring the structure of the Pd islands for extended time periods at RT.

■ EXPERIMENTAL SECTION

The experiments were performed in an ultrahigh vacuum chamber with a base pressure of 1×10^{-10} mbar, and the STM topographic images were all obtained at RT with an Omicron, GmbH, variable-temperature scanning probe microscope system. Images were acquired using Omicron MATRIX software, and data processing was performed using the WSxM program provided by Nanotech. 44 The Ag(111) and Au(111) surfaces were cleaned by repeated cycles of sputtering with argon (3 \times 10⁻⁵ mbar, 1000 V) and annealing to \sim 700 K. The surfaces were verified to be clean and well-ordered by lowenergy electron diffraction and STM. Palladium was deposited on Ag(111) and Au(111) via evaporation from a pure Pd rod (GoodFellow, 99.95%) using a triple electron beam evaporator (EFM 3T) with an integral flux monitor at a rate of 1×10^{-3} ML/s. The Pd coverage was determined directly from the STM images, and 1 ML corresponds to the Ag(111) and Au(111) atom densities of 1.38×10^{15} and 1.39×10^{15} atoms/

cm², respectively. During Pd evaporation, the Ag(111) and Au(111) surfaces were held at RT, and the background pressure never exceeded 3×10^{-10} mbar. For the annealing experiments, after Pd deposition, the surface was heated to the first target temperature and held there for 30 s, before cooling back to RT where the images were acquired. The annealing process generally took about 10 min. For the same Pd deposition, the sample was then heated to the next temperature, and the process was repeated.

RESULTS

Pd/Ag(111) and Pd/Au(111) at RT. Figure 1 shows STM images of clean (a) Ag(111) and (b) Au(111) surfaces

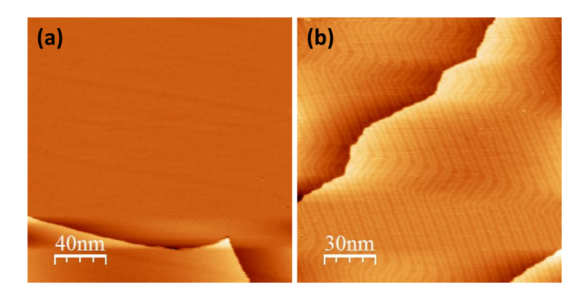


Figure 1. (a) Clean Ag(111) and (b) clean Au(111) surfaces with monolayer step edges and wide terraces. $22 \times \sqrt{3}$ reconstruction on Au(111) is clearly visible in (b). Images were acquired at 0.2 nA, 1.0–1.2 V.

confirming the well-known fact that although Au(111) undergoes a $22 \times \sqrt{3}$ (herringbone) reconstruction, Ag(111) retains the ideal (111) structure and therefore features flat terraces separated by monatomic steps. Figure 2

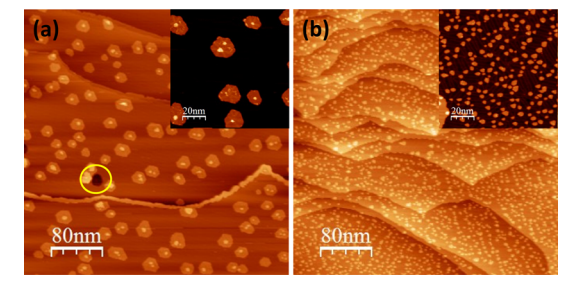


Figure 2. STM images of (a) 0.15 ML of Pd on Ag(111) and (b) 0.18 ML of Pd on Au(111) in a $400 \times 400 \text{ nm}^2$ area. Insets show the Pd islands on the terrace in a $100 \times 100 \text{ nm}^2$ area. Images were recorded at 0.20 nA, 2.0–1.0 V. A vacancy pit near Pd islands is shown in the yellow circle in (a).

shows STM topographic images of 0.15 ± 0.02 ML of Pd deposited on Ag(111) (a) and 0.18 ± 0.01 ML of Pd deposited on Au(111) (b) at RT. The roughly hexagonal-shaped Pd islands are distributed across the Ag terraces, and a distinct narrow band of intermediate height is seen along the step edge between the two Ag(111) terraces, as shown in Figure S1a. The appearance of the step edge in Figure S1a is similar to what Tierney et al. observed for Pd deposited onto Cu(111), which they termed an alloy brim. For Au(111), Pd islands with irregular shapes are distributed across the Au terrace with a limited amount of Pd alloyed at the step. Deposition of Pd does not lift the herringbone reconstruction, but it is not apparent in Figure 2b as the color contrast was

chosen to highlight the Pd islands. An image with a contrast that makes the herringbone reconstruction in the presence of Pd islands clearer is shown in Figure S2a. As shown in Figure S2a, the Pd islands mainly grew at the edge dislocations of the Au(111) surface, which accounts for the arrangement of many of the Pd islands along lines. This is consistent with previously reported Pd island nucleation on Au(111). 432-34 Bright features near the centers of most of the Pd islands are observed in Figure 2a on Ag(111). Previously, we reported that these bright features are due to Ag atoms nucleated in the middle of Pd islands. 16 Thus, Ag capping of the Pd islands on Ag(111) started from the center of the islands at RT. This kind of bright feature is not observed on the Pd islands on Au(111). Moreover, capping of the Pd islands on Ag(111) is accompanied by vacancy pit formation near the Pd islands, as shown in the yellow circle in Figure 2a. The growth of an Ag capping layer occurs both for Pd islands next to the vacancy pits and for Pd islands further away. This is attributed to a lower energy for growing an existing pit relative to forming a new pit. Some of the Ag atoms could have also come from detachment from steps or just from the small number of Ag adatoms that are always present on the terraces. Regardless of their origin, the observation of capping indicates a high mobility of Ag atoms on the surface at RT. In contrast, vacancy pit formation was not observed near the Pd islands on the Au(111) surface. The contrasting behavior on Ag(111) and Au(111) arises because the barrier for the pop-out of a substrate atom next to a Pd island is lower on Ag(111) than on Au(111). 16,46 Similarly, Bulou and Bucher found that a large activation energy is required to eject an Au atom close to a Co cluster in an STM study of Co on Au(111).²³

Despite the absence of vacancy pits, some two-layer islands are observed after Pd deposition on Au(111) at RT, as shown in Figure 3a. Only about 1% of the islands seen in Figure 2b

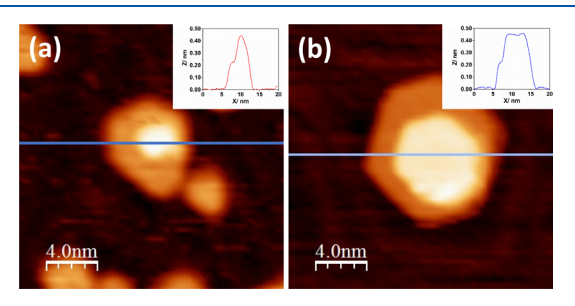


Figure 3. (a) STM image of a Pd island having a partially grown Au layer on Au(111) at RT. Inset shows the height profile along the blue line. (b) STM image of a different Pd island having a partially grown Au layer on Au(111) upon annealing to 440 K. Inset shows the height profile along the blue line. Height of the double-layer island is 0.45 ± 0.01 nm

have a second layer, and for images taken 24 h after Pd deposition, as shown in Figure 4b, the fraction of islands with a second layer only increases to 4%. Figure 3b is typical of many images in showing that the area of the second layer increases after annealing to 440 K. The height of the double layer island in Figure 3 is 0.45 ± 0.01 nm, whereas the monolayer Pd island's height on Au(111) is 0.20 ± 0.01 nm and the monoatomic step height of Au(111) is 0.24 ± 0.01 nm, suggesting that the double-layer islands consist of an Au layer on top of a Pd layer. For Ag(111), we reported the height of Ag-encapsulated Pd islands to be 0.420 nm and Patel et al.

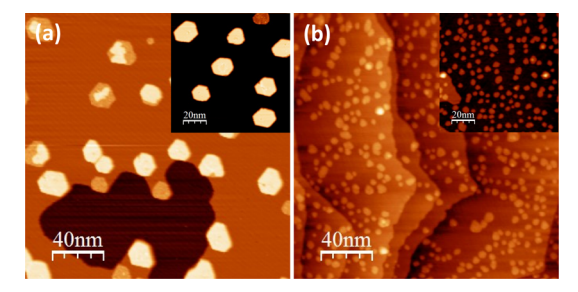


Figure 4. STM images of (a) Pd/Ag(111) and (b) Pd/Au(111) 24 h at RT after Pd deposition. Images were recorded at 0.20 nA, 2.0–1.0 V. Insets show the Pd islands on the terrace in a $100 \times 100 \text{ nm}^2$ area. Nearly 80% of Pd islands are covered by Ag atoms creating vacancy pits on Ag(111), whereas less than 4% of Pd islands are covered by Au atoms without creating vacancy pits on Au(111).

reported 0.459 nm high Ag-capped Pt-rich islands for Pt deposited on Ag(111). ^{16,47} However, we note that conclusions based on heights alone are not definitive as the Au–Pd interlayer interaction could make the height of a Au-capped Pd island different from what is expected based on assuming that layer heights are simply additive. Because the formation of the Au-capped Pd islands is not accompanied by the formation of vacancy pits, the Au atoms likely detach from step edges and diffuse onto the Pd islands. Because relatively few Au-capped islands are observed, distinct changes in the Au step edges would not be expected and were not observed.

Figure 4 shows that 24 h at RT after Pd deposition, $\sim 80\%$ of the Pd islands on Ag(111) are encapsulated, whereas less than 4% of the Pd islands are encapsulated on Au(111). The large dark area seen in Figure 4a is a vacancy pit that formed on the Ag(111) surface, whereas vacancy pit formation was not observed on the Au(111) surface even 24 h after Pd deposition. This indicates that bare monolayer Pd islands on the Au(111) surface retain their initial structure for an extended period, in contrast to Pd islands on Ag(111).

Effect of Annealing Temperature. Figures 5 and 6 show the evolution of the 0.15 ML Pd/Ag(111) and 0.18 ML Pd/Au(111) surfaces, respectively, with increasing annealing temperature. Larger scale images for Pd/Au(111) are given in Figure S3. Annealing the Ag(111) surface to 340 K gives rise to mainly Ag-encapsulated Pd islands accompanied by the creation of vacancy pits. A greater variety of island structures were observed upon annealing Pd on Ag(111), including three-layer islands with a composition of Ag/Ag/Pd/Ag(111) and double layer Ag islands on top of Pd islands that have receded into the Ag(111) surface. Further details on the different types of islands observed with annealing Pd/Ag(111) are given elsewhere. ¹⁶

In contrast to Ag(111), less than 4% of the Pd islands are encapsulated by Au upon annealing the Pd/Au(111) surface to 340 K. This indicates that Pd islands are more stable on Au(111) than on Ag(111) not only at RT but also at 340 K. We did not observe a wide variety of island structures on Au(111) upon annealing. Pd diffused into the Au(111) subsurface upon further annealing to 470 K. Figure 7 shows histograms of the areas of the Pd islands (Figure 7a) and the island density (Figure 7b) after annealing Pd/Au(111). The islands increased in size and their density decreased with increasing annealing temperature. Most importantly, annealing caused extensive vacancy pit formation on Pd/Ag(111), but not on Pd/Au(111).

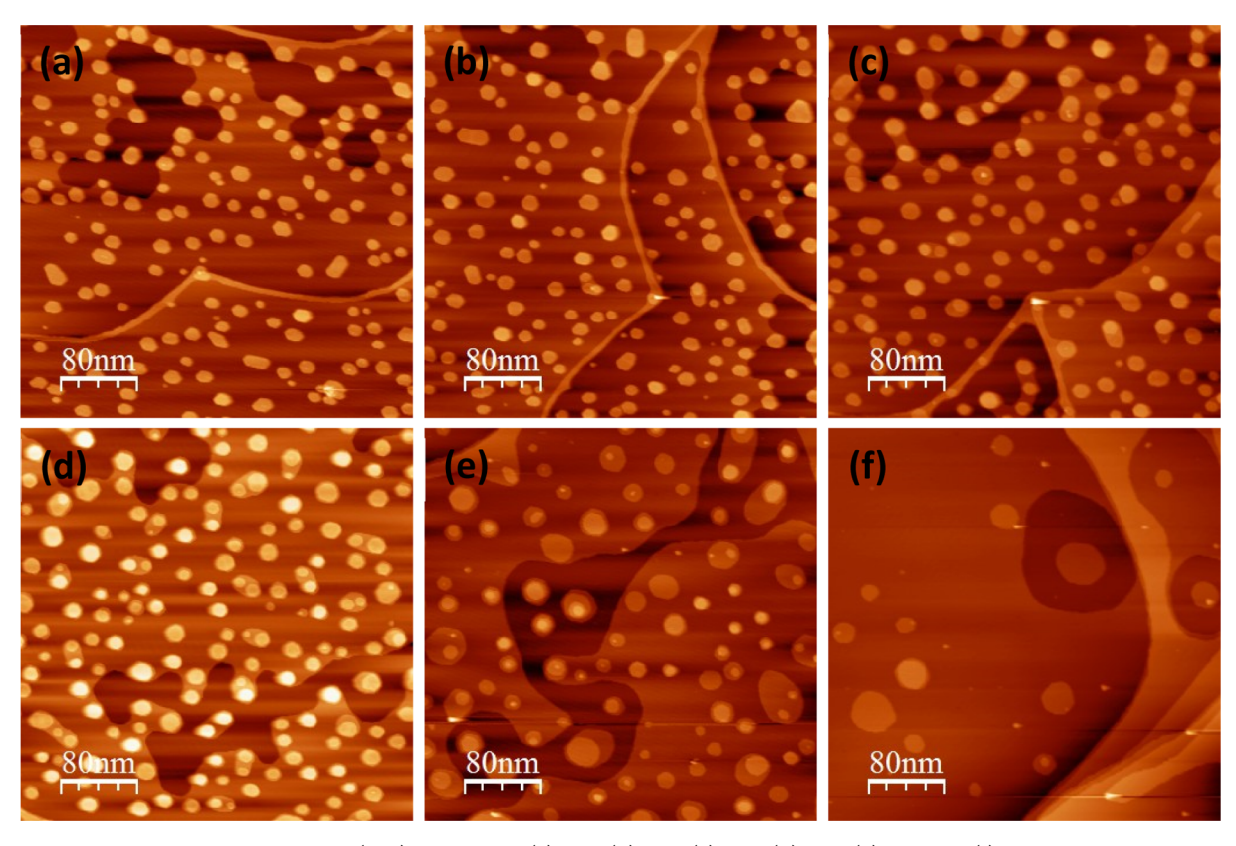


Figure 5. STM images of 0.15 ML Pd on Ag(111) annealed to (a) 340, (b) 390, (c) 420, (d) 440, (e) 450, and (f) 470 K. Images were recorded at 0.20 nA, 1.0 V. Area of the images is $400 \times 400 \text{ nm}^2$.

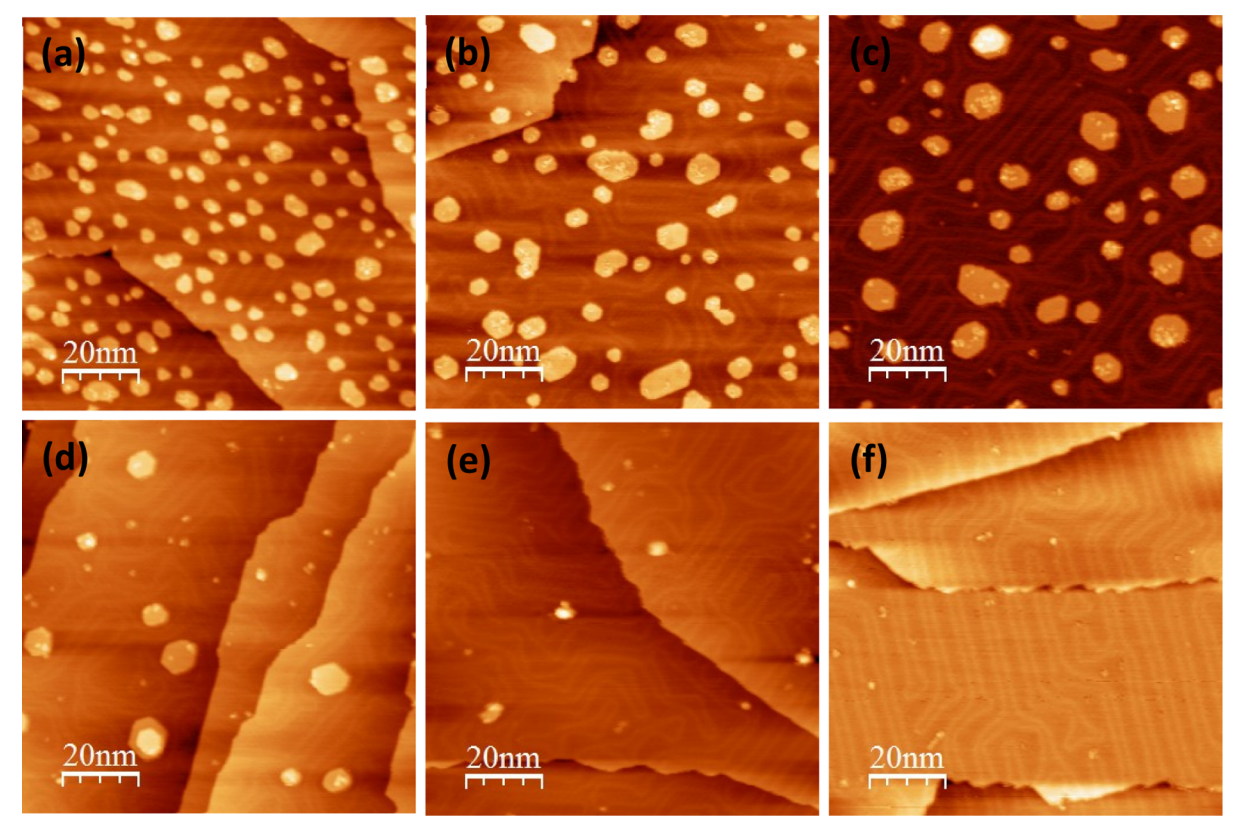


Figure 6. STM images of 0.18 ML Pd on Au(111) annealed to (a) 340, (b) 390, (c) 420, (d) 440, (e) 450, and (f) 470 K. Images were recorded at 0.20 nA, 1.0 V. Area of the images is $100 \times 100 \text{ nm}^2$. See Figure S3 in the Supporting Information for the images of the $300 \times 300 \text{ nm}^2$ area.

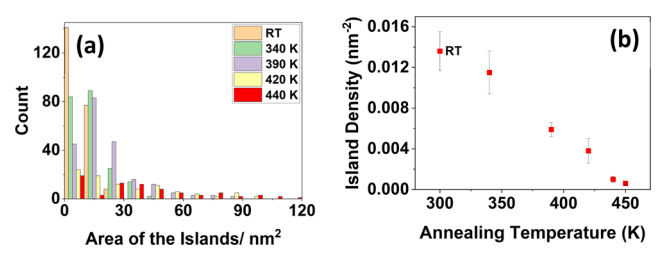


Figure 7. (a) Histograms of the areas of Pd islands on the Au(111) surface at RT and after annealing to 340, 390, 420, and 440 K. (b) Plot of island density vs annealing temperature.

DISCUSSION

Pd/Ag(111) and Pd/Au(111) at RT. The different behaviors of Pd on the Ag(111) and Au(111) surfaces following RT deposition reflect the different structures of the two clean surfaces, as revealed in Figure 1. Although the Ag(111) terraces appear flat and featureless, Au(111) has the well-known 22 $\times \sqrt{3}$ reconstruction (herringbone) structure. 48-52 This structure features a periodic arrangement of ridges and elbows, and previous work has shown that the elbows provide nucleation sites for island growth for many metals deposited onto Au(111). In the case of Pd, Stephenson et al. and Casari et al. have studied the nucleation and growth of Pd islands on Au(111) at RT with STM. 33,34 Stephenson et al. reported that the herringbone reconstruction is relatively undisturbed at low Pd coverages but is distorted at higher Pd coverages.³³ Casari et al. proposed that place exchange of Pd atoms at the elbow sites is responsible for ordered nucleation of Pd islands on Au(111).³⁴ Baber et al. obtained atomically resolved images with low-temperature STM of Pd atoms embedded in the topmost Au layer near the elbow region and also confirmed that RT Pd deposition leads to islands nucleated at the herringbone elbows. 4,35 Our results are consistent with these previous reports. In Figure 2b, it appears that the Pd islands on Au(111) are not randomly distributed but follow lines determined by the elbows in the herringbone structure. Further evidence of this is presented in Figure S2b,c, which shows that Pd islands form only on wide terraces containing dislocation line elbows but not on narrow terraces lacking such elbows. Furthermore, the small size and higher island density on Au(111) relative to Ag(111) reflect the higher binding energy of Pd atoms at the nucleation sites of Au(111) so that once a Pd atom attaches to those sites, they lose the high mobility needed to form the larger islands seen on Ag(111), which lacks such higher binding energy sites. As shown in Figure S4, this results in an average Pd island area of $260 \pm 87 \text{ nm}^2 \text{ on Ag}(111)$, but only $9.4 \pm 4.7 \text{ nm}^2 \text{ on}$ Au(111). The binding energy of Pd at the elbow sites is evidently stronger than that at the Au steps as unlike Ag(111), no accumulation of Pd at the Au(111) step sites is observed (Figure S1b). Recently, the dynamics of CO-induced restructuring of the Pd/Au(111) surface was studied with reflection absorption infrared spectroscopy, ab initio thermodynamics, and machine learning molecular dynamics (MD) simulations.⁵³ The MD simulations showed that at 600 K, a Pd₀₁ island on an unreconstructed Au(111) surface became encapsulated by Au atoms and then partially dissolved into the bulk leaving behind Pd monomers on the surface and vacancy pits. They did not investigate if different simulation results would have been obtained if the Pd₉₁ island had been placed on an Au(111) surface with the herringbone structure. Since

we did not achieve atomic resolution in our RT STM images, we would not have been able to detect isolated Pd atoms in the present study.

Effect of Annealing Temperature. We speculate that there are basically three processes that occur that are responsible for the changes in the Pd island structures on Au(111) that we observed as a function of annealing temperature. The first is Ostwald ripening in which Pd atoms detach from small islands and reattach to larger islands. The shift in the distribution toward larger islands is most apparent in comparing Figure 2b with Figures 6 and 7 after annealing Pd/Au(111) to 340 and 390 K. The second process is the migration of Pd into the Au subsurface, which leads to a clear decrease in the amount of Pd contained in islands for annealing temperatures of 440 K and above. Both the growth of larger islands at the expense of smaller ones and diffusion into the subsurface region contribute to the decrease in island density displayed in Figure 7b. Evidence for Pd diffusion into the bulk comes not only from STM images such as in Figures 5f and 6f but also from IR studies of adsorbed CO on Pd/ Ag(111)¹⁴ and Pd/Au(111).⁵³ As CO only adsorbs at RT on Pd sites, but not on Ag or Au sites, the disappearance with annealing of the peak corresponding to CO adsorbed on Pd atoms demonstrates that Pd has disappeared from the surface. The third process is the exchange of Pd for Au, which can change the composition of the deposited Pd islands into a PdAu alloy. Surface alloy formation was clearly revealed in a combined Auger electron spectroscopy, X-ray photoelectron spectroscopy, and low-energy ion scattering spectroscopy study of Pd films on Au(111) by Koel et al.⁵⁴ A process that readily occurs on Pd/Ag(111) but only to a very small extent on Pd/Au(111) is encapsulation of the Pd islands by a second layer of host atoms. The Ag-capped Pd islands do not increase in size for annealing temperatures up to 450 K as the presence of the Ag atoms stabilizes against detachment of Pd atoms from the islands, which is necessary for Ostwald ripening to occur. Above 450 K, Ag islands remain after the underlying Pd atoms diffuse into the subsurface or form a surface alloy, and these Ag islands grow for annealing temperatures of 450 K and above. To distinguish Pd from Au or Ag atoms within the islands using STM would require atomically resolved images with very low noise levels, something that is generally not possible for imaging at RT. Thus, our discussion of the atomicscale processes that occur in these two systems is somewhat speculative.

Vacancy Pit Formation. The vacancy pits that are observed to accompany encapsulation of Pd islands by Ag atoms on Ag(111) are not observed for Pd islands on Au(111). The herringbone reconstruction evidently confers extra stability to the Au atoms of the Au(111) surface and increases the energy required to move Au atoms to the top of the Pd islands, despite the lower surface free energy of Au relative to Pd. Furthermore, the dislocation lines on Au(111) are quite mobile and readily respond to the presence of the deposited Pd atoms. As observed in Figures 6 and S5, the dislocation lines tend to wrap around the islands, as has been reported in previous studies. A,33,34,55 The rearrangement of the dislocations on the Au(111) surface in response to the Pd islands further stabilizes the Au surface atoms to make the activation energy for encapsulation higher for Pd on Au(111) than on Ag(111).

CONCLUSIONS

Surface free energies provide a simple way to predict the composition of bimetallic surfaces with the topmost atomic layer enriched in the element with the lower surface free energy. Thus, the lower surface free energies of Ag and Au correctly predict that Pd deposited onto Ag and Au surfaces will diffuse into the subsurface at temperatures high enough to overcome the relevant activation energies. However, for Pd deposited at RT, the structures observed are limited by the kinetics of the processes involved. Despite the similar properties of Ag and Au, their (111) surfaces have distinctly different structures. On the unreconstructed Ag(111) surface, the formation of relatively large two-dimensional Pd islands can be attributed to a large mean free path of the deposited Pd atoms allowing the atoms to attach to already nucleated Pd islands. In contrast, the $22 \times \sqrt{3}$ (herringbone) reconstruction of Au(111) provides a high density of nucleation sites, implying that the spacing of these sites is less than the mean free path of the deposited Pd atoms such that much smaller islands are observed compared to Ag(111). Furthermore, the activation energy for migration of Au atoms to the top of Pd islands on Au(111) is high enough that encapsulation of Pd islands along with vacancy pit formation is not observed, in marked contrast to Pd deposited onto Ag(111). The results presented here illustrate that general thermodynamic principles are insufficient for predicting the detailed structural properties of bimetallic surfaces and that the structure of each bimetallic pair must be investigated on a case-by-case basis.

ASSOCIATED CONTENT

Supporting Information

The Supporting Information is available free of charge at https://pubs.acs.org/doi/10.1021/acs.jpcc.2c05386.

Additional STM images obtained under different conditions for Pd on both Ag(111) and Au(111) (PDF)

AUTHOR INFORMATION

Corresponding Author

Michael Trenary — Department of Chemistry, University of Illinois at Chicago, Chicago, Illinois 60607, United States; orcid.org/0000-0003-1419-9252; Phone: 312 996-0777; Email: mtrenary@uic.edu; Fax: 312 996-0431

Author

Buddhika S. A. Gedara — Department of Chemistry, University of Illinois at Chicago, Chicago, Illinois 60607, United States; © orcid.org/0000-0002-4275-7621

Complete contact information is available at: https://pubs.acs.org/10.1021/acs.jpcc.2c05386

Notes

The authors declare no competing financial interest.

ACKNOWLEDGMENTS

The authors thank Prof. Nan Jiang for providing the Ag and Au samples and Dr. Linfei Li and Dairong Liu for assistance with the operation and maintenance of the STM system. The authors gratefully acknowledge financial support from the National Science Foundation (CHE-2102622).

REFERENCES

- (1) Kesavan, L.; et al. Solvent-Free Oxidation of Primary Carbon-Hydrogen Bonds in Toluene Using Au-Pd Alloy Nanoparticles. *Science* **2011**, 331, 195–199.
- (2) Maroun, F.; Ozanam, F.; Magnussen, O. M.; Behm, R. J. The Role of Atomic Ensembles in the Reactivity of Bimetallic Electrocatalysts. *Science* **2001**, 293, 1811–1814.
- (3) Bonarowska, M.; Malinowski, A.; Juszczyk, W.; Karpiński, Z. Hydrodechlorination of CCl₂F₂ (CFC-12) over silica-supported palladium-gold catalysts. *Appl. Catal. B Environ.* **2001**, *30*, 187–193.
- (4) Baber, A. E.; Tierney, H. L.; Lawton, T. J.; Sykes, E. C. H. An Atomic-Scale View of Palladium Alloys and Their Ability to Dissociate Molecular Hydrogen. *ChemCatChem* **2011**, *3*, 607–614.
- (5) Ouyang, M.; Papanikolaou, K. G.; Boubnov, A.; Hoffman, A. S.; Giannakakis, G.; Bare, S. R.; Stamatakis, M.; Flytzani-Stephanopoulos, M.; Sykes, E. C. H. Directing Reaction Pathways via In situ Control of Active Site Geometries in PdAu Single-Atom Alloy Catalysts. *Nat. Commun.* **2021**, *12*, 1549.
- (6) Muir, M.; Molina, D. L.; Islam, A.; Abdel-Rahman, M. K.; Trenary, M. Selective Hydrogenation of Acrolein on a Pd/Ag(111) Single-Atom Alloy Surface. *J. Phys. Chem. C* **2020**, *124*, 24271–24278.
- (7) Aich, P.; Wei, H.; Basan, B.; Kropf, A. J.; Schweitzer, N. M.; Marshall, C. L.; Miller, J. T.; Meyer, R. Single-Atom Alloy Pd-Ag Catalyst for Selective Hydrogenation of Acrolein. *J. Phys. Chem. C* **2015**, *119*, 18140–18148.
- (8) Ding, Y.; Sun, W.; Yang, W.; Li, Q. Formic acid as the in-situ hydrogen source for catalytic reduction of nitrate in water by PdAg alloy nanoparticles supported on amine-functionalized SiO₂. *Appl. Catal. B Environ.* **2017**, 203, 372–380.
- (9) Troutman, J. P.; Li, H.; Haddix, A. M.; Kienzle, B. A.; Henkelman, G.; Humphrey, S. M.; Werth, C. J. PdAg Alloy Nanocatalysts: Toward Economically Viable Nitrite Reduction in Drinking Water. *ACS Catal.* **2020**, *10*, 7979–7989.
- (10) Lu, Y.; Chen, W. PdAg Alloy Nanowires: Facile One-Step Synthesis and High Electrocatalytic Activity for Formic Acid Oxidation. ACS Catal. 2012, 2, 84–90.
- (11) Mori, K.; Sano, T.; Kobayashi, H.; Yamashita, H. Surface Engineering of a Supported PdAg Catalyst for Hydrogenation of CO2 to Formic Acid: Elucidating the Active Pd Atoms in Alloy Nanoparticles. J. Am. Chem. Soc. 2018, 140, 8902–8909.
- (12) Xu, L.; Cui, T.; Zhu, J.; Wang, X.; Ji, M. PdAg alloy nanoparticles immobilized on functionalized MIL-101-NH₂: effect of organic amines on hydrogenation of carbon dioxide into formic acid. *New J. Chem.* **2021**, *45*, *62*93–6300.
- (13) Singh, A. K.; Hwang, Y.-H.; Kim, D.-P. Heterogeneous PdAg Alloy Catalyst for Selective Methylation of Aromatic Amines with Formic Acid under An Additive-Free and Solvothermal One-Pot Condition. NPG Asia Mater. 2015, 7, No. e222.
- (14) Muir, M.; Trenary, M. Adsorption of CO to Characterize the Structure of a Pd/Ag(111) Single-Atom Alloy Surface. *J. Phys. Chem.* C **2020**, *124*, 14722–14729.
- (15) O'Connor, C. R.; Duanmu, K.; Patel, D. A.; Muramoto, E.; van Spronsen, M. A.; Stacchiola, D.; Sykes, E. C. H.; Sautet, P.; Madix, R. J.; Friend, C. M. Facilitating hydrogen atom migration via a dense phase on palladium islands to a surrounding silver surface. *Proc. Natl. Acad. Sci. U.S.A.* **2020**, *117*, 22657–22664.
- (16) Gedara, B. S. A.; Muir, M.; Islam, A.; Liu, D.; Trenary, M. Room Temperature Migration of Ag Atoms to Cover Pd Islands on Ag(111). *J. Phys. Chem. C* **2021**, *125*, 27828–27836.
- (17) Mezey, L. Z.; Giber, J. The Surface Free Energies of Solid Chemical Elements: Calculation from Internal Free Enthalpies of Atomization. *Jpn. J. Appl. Phys.* **1982**, *21*, 1569–1571.
- (18) Kuntze, J.; Speller, S.; Heiland, W.; Deurinck, P.; Creemers, C.; Atrei, A.; Bardi, U. Surface structure and segregation profile of the alloyAu₃Pd(110):Experiment and theory. *Phys. Rev. B: Condens. Matter Mater. Phys.* **1999**, *60*, 9010–9018.
- (19) Christensen, A.; Ruban, A. V.; Stoltze, P.; Jacobsen, K. W.; Skriver, H. L.; Nørskov, J. K.; Besenbacher, F. Phase diagrams for

- surface alloys. Phys. Rev. B: Condens. Matter Mater. Phys. 1997, 56, 5822-5834.
- (20) Giesen, M. Step and island dynamics at solid/vacuum and solid/liquid interfaces. *Prog. Surf. Sci.* **2001**, *68*, 1–154.
- (21) Peale, D. R.; Cooper, B. H. Adsorbate-promoted mass flow on the gold (111) surface observed by scanning tunneling microscopy. *J. Vac. Sci. Technol., A* **1992**, *10*, 2210–2215.
- (22) Spurgeon, P. M.; Lai, K. C.; Han, Y.; Evans, J. W.; Thiel, P. A. Fundamentals of Au(111) Surface Dynamics: Coarsening of Two-Dimensional Au Islands. *J. Phys. Chem. C* **2020**, *124*, 7492–7499.
- (23) Bulou, H.; Bucher, J.-P. Long Range Substrate Mediated Mass Transport on Metal Surfaces Induced by Adatom Clusters. *Phys. Rev. Lett.* **2006**, *96*, 076102.
- (24) Rai, A.; Nayak, J.; Roy Barman, S. Chromium Nano-Islands on Au(111). e-J. Surf. Sci. Nanotechnol. 2014, 12, 49–52.
- (25) Stroscio, J. A.; Pierce, D. T.; Dragoset, R. A.; First, P. N. Microscopic Aspects of the Initial Growth of Metastable fcc Iron on Au(111). J. Vac. Sci. Technol., A 1992, 10, 1981–1985.
- (26) Fonin, M.; Dedkov, Y. S.; Rüdiger, U.; Güntherodt, G. Growth and structure of Mn on Au(111) at room temperature. *Surf. Sci.* **2003**, 529, L275–L280.
- (27) Biener, M. M.; Biener, J.; Schalek, R.; Friend, C. M. Surface alloying of immiscible metals: Mo on Au(111) studied by STM. *Surf. Sci.* **2005**, *594*, 221–230.
- (28) Chambliss, D. D.; Wilson, R. J.; Chiang, S. Ordered Nucleation of Ni and Au Islands on Au(111) Studied by Scanning Tunneling Microscopy. J. Vac. Sci. Technol., B: Microelectron. Nanometer Struct.–Process., Meas., Phenom. 1991, 9, 933–937.
- (29) Chambliss, D. D.; Wilson, R. J.; Chiang, S. Nucleation of ordered Ni island arrays on Au(111) by surface-lattice dislocations. *Phys. Rev. Lett.* **1991**, *66*, 1721–1724.
- (30) Trant, A. G.; Jones, T. E.; Gustafson, J.; Noakes, T. C. Q.; Bailey, P.; Baddeley, C. J. Alloy formation in the Au{111}/Ni system An investigation with scanning tunnelling microscopy and medium energy ion scattering. *Surf. Sci.* **2009**, *603*, 571–579.
- (31) Wang, Z. T.; Darby, M. T.; Therrien, A. J.; El-Soda, M.; Michaelides, A.; Stamatakis, M.; Sykes, E. C. H. Preparation, Structure, and Surface Chemistry of Ni-Au Single Atom Alloys. *J. Phys. Chem. C* **2016**, *120*, 13574–13580.
- (32) Wu, C.; Xu, F.; Castell, M. R.; Tsang, S. C. E. The effect of the size of surface Pd island ensembles on electron transfer of adsorbed perchlorate ions on Au(111). *Chem. Commun.* **2014**, *50*, 1198–1201.
- (33) Stephenson, A. W.; Baddeley, C. J.; Tikhov, M. S.; Lambert, R. M. Nucleation and growth of catalytically active Pd islands on Au(111)-22 × studied by scanning tunnelling microscopy. *Surf. Sci.* **1998**, 398, 172–183.
- (34) Casari, C. S.; Foglio, S.; Siviero, F.; Li Bassi, A.; Passoni, M.; Bottani, C. E. Direct observation of the basic mechanisms of Pd island nucleation on Au(111). *Phys. Rev. B: Condens. Matter Mater. Phys.* **2009**, *79*, 195402.
- (35) Baber, A. E.; Tierney, H. L.; Sykes, E. C. H. Atomic-Scale Geometry and Electronic Structure of Catalytically Important Pd/Au Alloys. *ACS Nano* **2010**, *4*, 1637–1645.
- (36) Pedersen, M. Ø.; Helveg, S.; Ruban, A.; Stensgaard, I.; Lægsgaard, E.; Nørskov, J. K.; Besenbacher, F. How a gold substrate can increase the reactivity of a Pt overlayer. *Surf. Sci.* **1999**, 426, 395–400
- (37) Altman, E. I.; Colton, R. J. Growth of Rh on Au(111): surface intermixing of immiscible metals. *Surf. Sci.* **1994**, *304*, L400–L406.
- (38) Chado, I.; Scheurer, F.; Bucher, J. P. Absence of ferromagnetic order in ultrathin Rh deposits grown under various conditions on gold. *Phys. Rev. B: Condens. Matter Mater. Phys.* **2001**, *64*, 094410.
- (39) Kang, J.; Rui, N.; Rosales, R.; Tian, Y.; Senanayake, S. D.; Rodriguez, J. A. Understanding the Surface Structure and Catalytic Activity of SnO_x/Au(111) Inverse Catalysts for CO₂ and H₂ Activation. *J. Phys. Chem. C* **2022**, *126*, 4862–4870.
- (40) Biener, J.; Farfan-Arribas, E.; Biener, M.; Friend, C. M.; Madix, R. J. Synthesis of TiO₂ nanoparticles on the Au(111) surface. *J. Chem. Phys.* **2005**, 123, 094705.

- (41) Schüttler, K. M.; Bansmann, J.; Engstfeld, A. K.; Behm, R. J. Low-temperature nucleation and growth of Zn on Au(111) and thermal stability toward (surface) alloy formation. *J. Chem. Phys.* **2021**, *155*, 124704.
- (42) Schüttler, K. M.; Bansmann, J.; Engstfeld, A. K.; Behm, R. J. Adlayer Growth vs Spontaneous (Near-) Surface Alloy Formation: Zn Growth on Au(111). *J. Chem. Phys.* **2020**, *152*, 124701.
- (43) van Spronsen, M. A.; Daunmu, K.; O'Connor, C. R.; Egle, T.; Kersell, H.; Oliver-Meseguer, J.; Salmeron, M. B.; Madix, R. J.; Sautet, P.; Friend, C. M. Dynamics of Surface Alloys: Rearrangement of Pd/Ag(111) Induced by CO and O₂. *J. Phys. Chem. C* **2019**, *123*, 8312–8323.
- (44) Horcas, I.; Fernandez, R.; Gómez-Rodríguez, J. M.; Colchero, J.; Gómez-Herrero, J.; Baro, A. M. WSXM: A software for scanning probe microscopy and a tool for nanotechnology. *Rev. Sci. Instrum.* **2007**, *78*, 013705.
- (45) Tierney, H. L.; Baber, A. E.; Sykes, E. C. H. Atomic-Scale Imaging and Electronic Structure Determination of Catalytic Sites on Pd/Cu Near Surface Alloys. *J. Phys. Chem. C* **2009**, *113*, 7246–7250.
- (46) Lim, J. S.; et al. Evolution of Metastable Structures at Bimetallic Surfaces from Microscopy and Machine-Learning Molecular Dynamics. *J. Am. Chem. Soc.* **2020**, *142*, 15907–15916.
- (47) Patel, D. A.; Kress, P. L.; Cramer, L. A.; Larson, A. M.; Sykes, E. C. H. Elucidating the composition of PtAg surface alloys with atomic-scale imaging and spectroscopy. *J. Chem. Phys.* **2019**, *151*, 164705.
- (48) Wang, Y.; Hush, N. S.; Reimers, J. R. Simulation of the $Au(111)-(22\times\sqrt{3})$ surface reconstruction. *Phys. Rev. B: Condens. Matter Mater. Phys.* **2007**, 75, 233416.
- (49) Bulou, H.; Goyhenex, C. Local Strain Analysis of the Herringbone Reconstruction of Au(111) through Atomistic Simulations. *Phys. Rev. B: Condens. Matter Mater. Phys.* **2002**, *65*, 045407.
- (50) Takeuchi, N.; Chan, C. T.; Ho, K. M. Au(111): A Theoretical Study of the Surface Reconstruction and the Surface Electronic Structure. *Phys. Rev. B: Condens. Matter Mater. Phys.* **1991**, 43, 13899–13906.
- (51) Barth, J. V.; Brune, H.; Ertl, G.; Behm, R. J. Scanning Tunneling Microscopy Observations on the Reconstructed Au(111) Surface: Atomic Structure, Long-Range Superstructure, Rotational Domains, and Surface Defects. *Phys. Rev. B: Condens. Matter Mater. Phys.* 1990, 42, 9307–9318.
- (52) Wöll, C.; Chiang, S.; Wilson, R. J.; Lippel, P. H. Determination of Atom Positions at Stacking-Fault Dislocations on Au(111) by Scanning Tunneling Microscopy. *Phys. Rev. B: Condens. Matter Mater. Phys.* **1989**, 39, 7988–7991.
- (53) Zhou, C.; Ngan, H. T.; Lim, J. S.; Darbari, Z.; Lewandowski, A.; Stacchiola, D. J.; Kozinsky, B.; Sautet, P.; Boscoboinik, J. A. Dynamical Study of Adsorbate-Induced Restructuring Kinetics in Bimetallic Catalysts Using the PdAu(111) Model System. *J. Am. Chem. Soc.* **2022**, *144*, 15132–15142.
- (54) Koel, B. E.; Sellidj, A.; Paffett, M. T. Ultrathin films of Pd on Au(111): Evidence for surface alloy formation. *Phys. Rev. B: Condens. Matter Mater. Phys.* **1992**, *46*, 7846–7856.
- (55) Hasegawa, Y.; Avouris, P. Manipulation of the Reconstruction of the Au(111) Surface with the STM. Science 1992, 258, 1763–1765.